



Original Article

# Aqueous *Cissus quadrangularis* Stem Extract Integrated Biodegradable Tissue Engineering Scaffold Augments Early Biomimetic and Biomineralization *In Vitro*

Praseetha R. Nair<sup>1</sup>, S. Sreeja<sup>1</sup> and G. S. Sailaja<sup>\*1,2,3</sup>

<sup>1</sup>Department of Polymer Science and Rubber Technology, <sup>2</sup>Inter-University Centre for Nanomaterials and Devices (IUCND), <sup>3</sup>Centre of Excellence in Advanced Materials, Cochin University of Science and Technology, Kochi 682022, India

Received: 9 December 2021  
Accepted: 25 December 2022  
Published online: 30 June 2023

**Keywords:** biodegradable scaffold, biomimetic mineralization, biomineralization, *Cissus quadrangularis*, aqueous extract

Biodegradable tissue engineering scaffolds with tunable degradation, high biocompatibility, adequate mechanical strength and intrinsic biomineralization potential instigating biomimetic interactions with osteogenic cells have been well-received for effective bone-defect repair. This study demonstrates the early biomimetic as well as biomineralization of aqueous stem extract (WE) of *Cissus quadrangularis* (CQ) integrated natural scaffold composed of chitosan and collagen (CC) with a tunable degradation profile. Results demonstrate that the scaffold (CC-WE) synergistically contributes to its biomineralization, water absorption capacity and tunable degradation. The microporous CC-WE with an average pore size of  $43.13 \pm 13.59 \mu\text{m}$  attained complete swelling within 1h and maintained equilibrium swelling for 10 days and subsequently underwent controlled degradation (42.3% by day 60) under physiological pH and ambient temperature. Early biomimetic mineralization has been observed by SEM analysis after immersing CC-WE in simulated body fluid under biomimetic conditions for 7 days. In complementary, early biomineralization has been confirmed by Alizarin Red S (ARS) and von Kossa (VK) staining upon interaction with Human Osteosarcoma (HOS) cells for 7 days, viewed as respective coloured adduct formation. The findings, therefore, suggest innate biomineralization proficiency of CC-WE scaffold under a beneficial biological microenvironment to aid faster bone defect healing.

© (2023) Society for Biomaterials & Artificial Organs #20062222

## Introduction

In the biomimetic therapeutic approach, natural systems are being emulated to mimic the structural and biofunctional features, presenting revolutionary contributions to effective tissue regeneration. Indeed, a significant number of natural as well as synthetic materials have been explored for regenerative tissue engineering by biomimetic approaches, including organic/inorganic matrices to augment biomineralization, a distinctive feature of osteogenesis [1, 2]. Such mineralized materials could function as superior matrices to facilitate a better cell-material interface triggering enhanced cell attachment, proliferation, and differentiation by promoting extracellular microarchitecture functions and simultaneously eliminating unfavourable cellular responses [3]. In particular, the cellular and molecular level interactions would be

key factors for the primary osteo-supportive microenvironment that leads to osteogenesis, thereby rectifying the bone defects.

The predominant requisites for a biomimetic bone graft essentially entail a hierarchically porous microstructure resembling the innate bone tissue microenvironment, a higher degree of compatibility with specific cells, controlled biodegradability to function as the supportive temporary extracellular matrix and invoke biomineralization of apatite with Ca/P ratio analogous to the stoichiometric ratio of host bone [1, 4]. Inspired by the natural mineralization process, collagen-based systems with diverse biological characteristics have been extensively used as tissue engineering scaffolds [5, 6].

The structural similarities with glycosaminoglycan and its biodegradable nature enable chitosan, the natural biocompatible polysaccharide, to function as a structural component of therapeutic tissue regeneration scaffolds [7]. Besides, it enhances the activity of growth factors to promote cell proliferation [7]. Moreover,

\* Corresponding author  
E-mail address: sailajags@cusat.ac.in (Dr. G.S. Sailaja)

chitosan is a cationic polyelectrolyte under acidic pH, contributed by its protonating primary amine groups, which leads to the formation of water-insoluble polyelectrolyte complexes with anionic substances [8]. Interestingly, collagen, a polyanionic fibrous protein that contains receptor-recognition repeats [9, 10], can form such ionic complexes with chitosan [8].

It is a vital factor to envisage that, in the native bone, the glycosaminoglycan in Extra Cellular Matrix (ECM) interweaves the fibrous structure of collagen to ensure mechanical stability to the bone tissue [7]. Hence, chitosan-collagen complex scaffolds could be expected to provide a favourable mechanical match with the host bone to be repaired and initiate osteogenic signals [7]. Furthermore, the chitosan-collagen scaffolds mimic the natural mineralization process and can act as an appropriate supportive platform to repair bone defects. [7]

Plants with medicinal significance are an enriched traditional resource, and extensive research is ongoing to investigate their active components towards formulating innovative therapeutic options [11]. *Cissus quadrangularis* Linn (CQ) is a perennial plant from the family *Vitaceae* with well-documented medicinal importance [12]. Various CQ stem extracts have extensively been investigated for osteoporotic defect repair and bone tissue regeneration applications [13,14]. Ethanolic CQ extract has been reported to induce bone regeneration in ovariectomized rats [13], while petroleum ether and hexane extracts of CQ have been investigated for their efficacy in bone fracture healing *in vitro* [14, 15]. We have recently reported a comparative evaluation of various extracts of CQ stem in augmenting biomineralization [16]. Our studies manifested that hexane and aqueous extracts have superior cell-proliferation and biomineralization index [17]. The therapeutic efficacy of these herbal medicines to invoke osteogenesis when combined with an appropriate supporting matrix in the form of a scaffold would complement each other for sustained functioning until the regeneration phase is complete.

Herein, we present a natural biodegradable bone scaffold, aqueous CQ stem extract (WE) integrated chitosan-collagen (CC), holding early biomimetic and biomineralization potential. Chitosan-collagen 75:25 (w/w) crosslinked with glyoxal has specifically been chosen owing to its optimum physico-chemical and mechanical characteristics, as per our recent study [16, 17]. The CC-WE scaffold has been evaluated for its physicochemical and morphological features, water absorption capacity and degradation behavior under physiological conditions. Subsequently, biocompatibility evaluation (MTT assay and actin-DAPI staining) and proficiency to induce Ca-P mineralization (in biomimetic conditions and after cell-scaffold interaction) were determined to present tangible evidence of matrix mineralization, a noticeable characteristic of a bone regenerative scaffold. The CC-WE demonstrates inherent early Ca-P mineralization, better cytocompatibility, hydrophilicity, and biodegradation; hence, it could be proposed as a suitable biofunctional scaffold for bone tissue repair and regeneration.

## Materials and Methods

All the reagents for Phosphate Buffered Saline (PBS), Simulated Body Fluid (SBF) [Sodium chloride (NaCl), Potassium chloride (KCl), Potassium dihydrogen phosphate ( $\text{KH}_2\text{PO}_4$ ), Di-sodium hydrogen phosphate dihydrate ( $\text{Na}_2\text{HPO}_4 \cdot 2\text{H}_2\text{O}$ ), Sodium bicarbonate ( $\text{NaHCO}_3$ ), Di-potassium hydrogen phosphate ( $\text{K}_2\text{HPO}_4$ ), Magnesium chloride hexahydrate ( $\text{MgCl}_2 \cdot 6\text{H}_2\text{O}$ ), Calcium chloride ( $\text{CaCl}_2$ ), Sodium sulphate ( $\text{Na}_2\text{SO}_4$ ), and Tris buffer] were procured from Sigma Aldrich, India. Cell culture media and its supplements were obtained from Gibco ThermoFisher

Scientific, India and Hi media, India. In addition, reagents and stains for biocompatibility and biofunctional assays were purchased from Sigma Aldrich, India. Silver nitrate was obtained from Spectrochem, India.

### Fabrication of CC and CC-WE scaffold

The CC scaffold has been fabricated as per the optimized procedure reported recently, where the chitosan-collagen ratio has been optimized as 75:25 for favourable physico-chemical and mechanical characteristics [17]. In a typical procedure, chitosan and collagen in the ratio (w/w) of 75:25 was mixed thoroughly and allowed to stir for 3h. Subsequently, 25 mg of WE were added to 10 mL of polymer solution; bath sonicated for 60 min and lyophilized for 48h. The lyophilized sample was then cross-linked with a 4% (v/v) glyoxal solution followed by a repeated lyophilization procedure for another 48h to obtain the CC-WE scaffold. The CC scaffold without WE served as the control of the study. Finally, the as-obtained scaffold was cut into square pieces (2 mm × 2 mm) for further analyses.

### Physico-chemical characterizations

The compositional evaluation of CC and CC-WE scaffolds was performed by ATR spectral analysis (PerkinElmer, UK), while surface morphology and microarchitecture analyses were carried out by Optical (Lawrence and Mayo, India) as well as Scanning Electron Microscopy (SEM; (JEOL Model, JSM-6390 LV, UK)).

### *In vitro* swelling and degradation studies

Swelling and degradation of the scaffolds were conducted in phosphate-buffered saline (1X PBS, pH 7.4) under ambient conditions. Briefly, the dry weight of the scaffolds ( $n = 3$ ) was recorded and then immersed in PBS solution (1X; pH 7.4) at 37°C. The medium was replenished every third day, and the weight of the scaffolds was measured at definite time intervals. The percentage of swelling was calculated as per equation (1). After 60 days of incubation, the scaffolds were dried at 37°C, and the percentage of degradation was calculated using equation (2).

$$\% \text{ Swelling} = [(w_1 - w_0)/w_0] \times 100 \quad (1)$$

( $w_0$  and  $w_1$  are dry and wet weights of the scaffolds, respectively).

$$\% \text{ degradation} = [(w_i - w_d)/w_i] \times 100 \quad (2)$$

( $w_i$  and  $w_d$  are the initial and final weights of the scaffolds, respectively).

### *In vitro* mineralization in SBF

The CC and CC-WE scaffolds were immersed in SBF (1.5X; pH 7.4) for determining the biomimetic mineralization potential of the scaffolds, according to the procedure reported elsewhere [18]. The scaffolds in SBF were incubated at 37°C for 14 days. The medium (SBF) was refreshed every alternative day to maintain the ionic concentration and pH of the medium intact. On days 7 and 14, the scaffolds were carefully collected, washed with Milli Q water, and dried at 37°C overnight. The Au-sputtered scaffolds were subjected to SEM analysis to gather information on the nucleation of apatite and mineralization features. The CC scaffolds treated in the same way served as control.

### MTT assay and Actin/DAPI staining

The biocompatibility of the scaffolds was evaluated using Human Osteosarcoma (HOS) cells (procured from NCCS, Pune, India) by MTT assay and Actin/DAPI staining. In brief, the HOS cells ( $1 \times 10^4$

cells/well) were cultured on the sterile scaffold ( $n = 3$ ) and placed in a 24-well plate provided with standard culture media and conditions. After 24h of incubation, an MTT assay was performed, and the absorbance of formazan crystals dissolved in DMSO was measured at 570 nm using Spark® Multimode Microplate Reader (Tecan, Switzerland). The percentage viability of the cells on the scaffolds with respect to the control (cells without scaffolds) was calculated. For Actin/DAPI staining, the cells ( $1 \times 10^4$  cells/well) were seeded into a 24-well plate on the sterile scaffold and incubated for 24h under standard culture conditions. After incubation, the cells were fixed with 4% (w/v) paraformaldehyde solution for 20 min, and Alexa fluor-488 Phalloidin was added to stain the F-actin filaments of the fixed cells followed by counterstaining with 4'6 diamidino-2-phenylindole (DAPI). The stained cells were observed under a phase-contrast inverted fluorescence microscope (Nikon Eclipse Ti2 Series, India).

#### Alizarin red S and von Kossa staining

Alizarin red S (ARS) and von Kossa staining methods were adopted to determine the innate Calcium Phosphate mineralization potential of the CC and CC-WE scaffolds [19, 20]. The HOS cells ( $1 \times 10^4$  cells/well) were seeded onto the sterile scaffolds in 24 well culture plates and incubated for 7 days by following standard cell culture conditions. After 7 days of incubation, the cells were fixed with 4% (w/v) paraformaldehyde solution for 20 min. For ARS staining, the fixed cells were washed multiple times with sterile

water followed by ARS (40mM; pH 4.1) staining for 30 min under gentle shaking. The cells were carefully washed with water, and the red-coloured deposition of Ca nodules was observed using a phase-contrast inverted microscope (Nikon Eclipse Ti2 Series, India). In the von Kossa staining procedure, the fixed cells were washed with cacodylate buffer and incubated with 5% (w/v) silver nitrate solution under UV light for half an hour and finally added 5% (w/v) sodium thiosulphate. The brownish to black deposition of phosphate was captured using a phase-contrast inverted microscope.

## Results and Discussions

### Physico-chemical and morphological characterizations of the scaffolds

The photographic and optical microscopic images provide preliminary information on the physical features of the scaffolds. The porous architecture of CC and CC-WE scaffolds is visible from optical micrographs [figure 1A (a-b)]. The yellowish colour of CC scaffold [figure 1A(a) (inset)] is transformed to intensified brown colour for CC-WE scaffolds due to the presence of WE [figure 1A(b) (inset)]. The characteristic peaks of chitosan and collagen in the CC-WE scaffold are affirmed from the ATR spectrum [figure 1B]. More specifically, the broad peak at  $3291 \text{ cm}^{-1}$  exemplifies -NH stretching vibrations of CC. Peaks observed at  $2941 \text{ cm}^{-1}$  and  $2864 \text{ cm}^{-1}$  represent asymmetric and symmetric stretching vibrations of the  $-\text{CH}_2$  group, while the presence of residual N-acetyl group

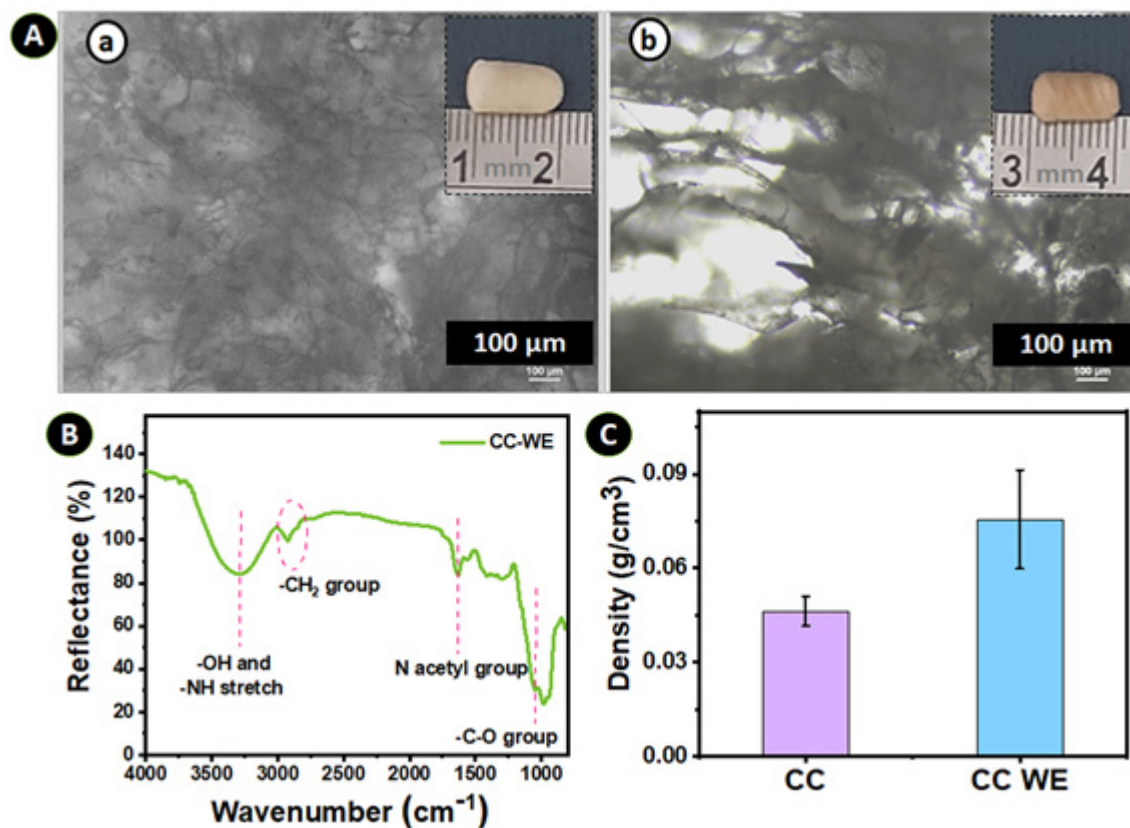
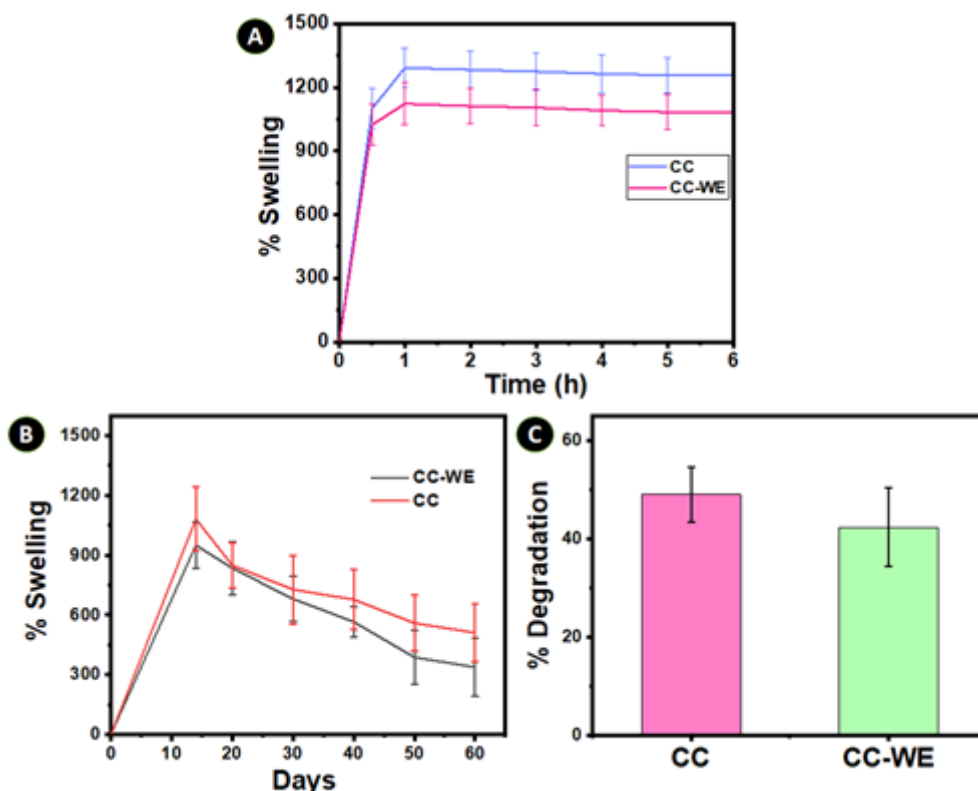


Figure 1: Physico-chemical characteristics and optical microscopic images of CC and CC-WE scaffolds, wherein A (a) and A (b) represent optical microscopic images of CC and CC-WE scaffold with photographs of the scaffolds as inset; (B) ATR spectrum and (C) density chart of CC and CC-WE scaffolds (all values are presented as mean  $\pm$  SD)



**Figure 2: Swelling behavior of CC and CC-WE scaffolds after (A) short term and (B) long term incubation in PBS; (C) degradation kinetics of scaffolds. All values are presented as mean  $\pm$  SD.**

was confirmed by the peak at  $1645\text{ cm}^{-1}$ . Additionally, the peak responsible for  $-\text{CO}$  stretching vibrations is noticed at  $1035\text{ cm}^{-1}$ . Density measurement data [figure 1C] indicate an increment in density for CC-WE ( $0.076 \pm 0.015\text{ g/cm}^3$ ) compared to CC scaffold ( $0.046 \pm 0.005\text{ g/cm}^3$ ), which is contributed by the presence of WE.

#### Water absorption and Degradation of CC-WE scaffold

The swelling and degradation profile of the scaffolds were investigated in biomimetic physiological conditions (figure 2A and B). Maximum swelling of CC and CC-WE scaffolds was obtained within 1h of incubation [figure 2A] in the medium and from there onwards a plateau is maintained for 10 days [figure 2B]. Thereafter, a drop in mass is observed for the scaffolds and is correlated to the preliminary phase of degradation, and an average weight reduction of 49% was recorded for CC and 42.3% for CC-WE on day 60 [figure 2C]. The swelling profile supports the suitability of the scaffolds for tissue regeneration applications. Precisely, the hydrophilic nature of the CC and CC-WE scaffold is crucial for cellular infiltration through the supportive three-dimensional matrix as well as for nutrient and metabolites transfer [21]. Apart from this, the increase in pore size and surface area/volume ratio of the scaffolds, due to controlled degradation, provide a better environment for the cells to infuse, attach and thereby enhance proliferation and differentiation [22]. Furthermore, the slow degradation of these scaffolds would deliver adequate support to the tissue until the repair phase completes [23].

Both CC and CC-WE exhibited microporous structure with open and closed cells evident from the SEM images [figure 3 A (a-b)], where the pore size is in the range of  $34.0$  to  $64.7\text{ }\mu\text{m}$  and  $23.4$  to

$64.4\text{ }\mu\text{m}$ , respectively. The inter-connected microporous arrangement of the scaffolds together with surface roughness provides a better platform for cellular infiltration [22,24], which would facilitate the cell-matrix interaction and initiate appropriate signaling to promote cell growth and proliferation [25]. It is well-known that the surface roughness enhances the nucleation and growth of apatite crystals [26]. Further, the amino groups of chitosan reinforce the triple helical structure of the collagen while cross-linking via dialdehyde, donated by glyoxal, significantly enables matrix integrity [27]. The EDX spectra of the scaffolds provided in figure 3A inset confirm the elements present in the system.

#### Biomimetic mineralization of scaffolds in SBF

Biomimetic mineralization in SBF provides preliminary insight into the bone-bonding ability of a three-dimensional tissue engineering matrix [18, 28]. The coherent apatite nucleation is apparent in SBF treated CC and CC-WE scaffolds (SEM micrographs) on days 7 and 14 [figure 3B and C]. The primary nucleation on the matrix (day 7) validates early mineralization [figure 3C (a)]. The thick layer of nodule-like mineralization, predominantly on CC-WE (day 14), provides clear evidence for the progression of nucleation to a secondary level, confirming the inherent biomimetic mineralization potential of CC-WE [figure 3C (b-c)]. A similar trend, but to a lesser extent, has been observed for the CC scaffold [figure 3B (b-c)]. The early mineralization witnessed in the CC-WE scaffold can be attributed to the synergistic effect of the chitosan-collagen and bioactive phytoconstituents of the WE containing nucleation sites and subsequently accelerating the mineralization process [29,30].

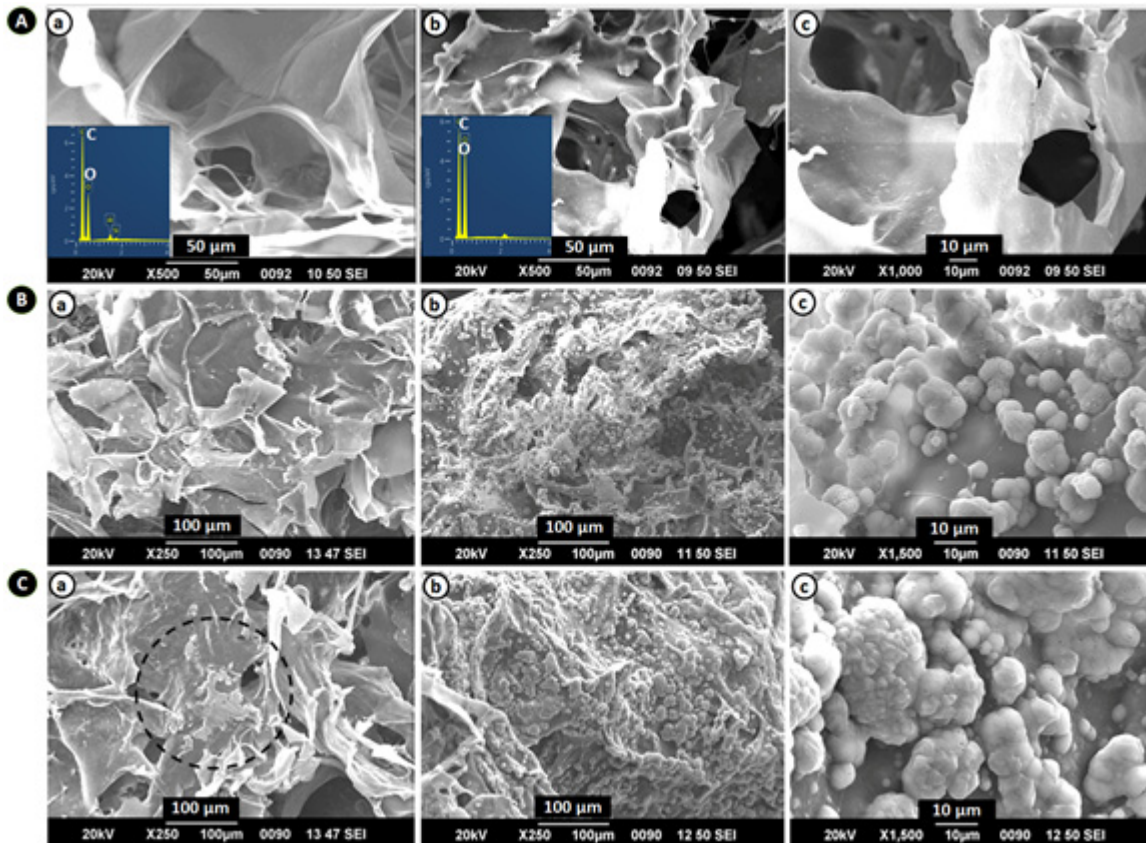


Figure 3: SEM images of the porous microarchitecture and biomimetic mineralization of CC and CC-WE scaffolds: Fig A (a) represents SEM images of the CC scaffold, A (b-c) represent the CC-WE scaffold at two different magnifications. Inset illustrates corresponding EDX spectrum. B(a) and C (a) represent SEM images of CC and CC-WE after 7 days of incubation in SBF, whereas B (b-c) and C (b-c) represent SEM images of CC and CC-WE scaffolds after 14 days of incubation at two different magnifications.

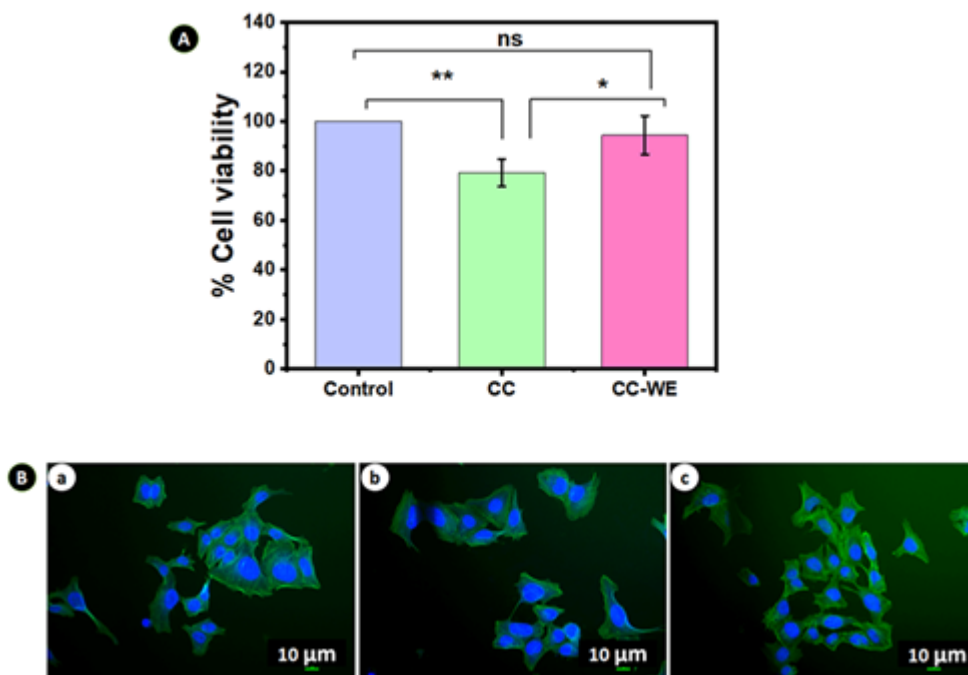


Figure 4: Cytocompatibility of CC and CC-WE scaffolds by (A) MTT assay and (B) Actin/DAPI staining [B(a-c) represent the control (no scaffold), CC and CC-WE respectively]. Note: Values are presented as mean  $\pm$  SD. 'ns' indicates non-significance with  $p > 0.05$ ; \* and \*\* indicate statistical significance with  $p$ -value  $< 0.05$  and  $< 0.01$ , respectively.

### Cytocompatibility evaluation of CC and CC-WE scaffold

The viability and morphological architecture of the cells demonstrated by MTT assay and F-actin/DAPI staining affirmed cytocompatibility of the CC-WE scaffold [figure 4]. The viability data from the MTT assay is presented as percentage cell viability in figure 4A, demonstrating CC-WE for a significantly high viability index ( $94.5\% \pm 7.7$ ), which is comparable to that of the control (untreated; no scaffold) cells, inferring the presence of metabolically active cells. Corroborative findings were noticed from Actin/DAPI staining as well [figure 4B]. The cells exhibited typical normal F-actin cytoskeleton morphology, indicating cytocompatibility of the scaffolds. Further supportive evidence was obtained from DAPI stained nuclei, where the nuclei remain intact analogous to the control cells after the cell-scaffold interactions. The elevated cytocompatibility of CC-WE originated from the synergistic effect of bioactive phytocomponents in the aqueous extract of CQ bound to the microporous CC scaffold presenting abundant availability of these components to interact with the cells and thereby, providing an adequate cellular microenvironment for adhesion and proliferation of the cells.

### Biom mineralization of CC-WE scaffolds

In general, an efficient bone tissue engineering scaffold should be capable of eliciting extracellular biomineralization while in contact with the cells [30]. The biomineralization potential of the scaffolds assessed by ARS and von Kossa staining following 7 days of cell-scaffold interaction is illustrated in figure 5. The ARS forms a red-colored complex with Ca nodules, while von Kossa staining produces a brownish to the black-colored product upon reaction with phosphate groups [19, 20], suggestive of biomineralization. An appreciable amount of red-colored Ca-ARS adduct was evident in the CC-WE scaffold [Fig. 5A(c)] and the cells incubated with CC scaffolds also showed Ca nodule formation, but less intense than

CC-WE [figure 5 A (b)]. Further, a higher degree of brownish-black deposition in CC-WE than CC after von Kossa staining portrays the cell-scaffold interaction triggered intense mineralization [figure 5 B]. The above observations clearly describe the innate capability of the CC-WE to persuade biomineralization, a remarkable feature of bone tissue regeneration.

The integration of WE to the natural CC scaffold refined the tissue regeneration behavior of the scaffold system by exploring the defined osteogenic potential of the individual components. As-fabricated CC-WE scaffold with well-distributed interconnected pores augmented the early biomimetic mineralization with added benefits on controlled degradation profile in the physiological condition, illustrating its suitability for bone tissue regeneration. Besides active components, the compatible cellular response due to suitable functional group, surface characteristics and morphological microarchitecture facilitated a better scaffold-cell interface subsequently invoked significant biomineralization.

### Conclusions

Recent decades witnessed a notable advancement in translational medicine, where traditional medicinal plants related knowledge are scientifically transformed into an established strategy with greater therapeutic potential. The present study demonstrates solid evidences of the early biomineralization potential of the aqueous CQ stem extract (WE) integrated chitosan-collagen hybrid scaffold. The porous micro-architecture and other surface features together with controlled degradation profile transformed the entire system (CC-WE) as an appropriate matrix, consequently facilitating better interaction with the cells, and thereby, augmented the aggregation of Ca-P minerals, a remarkable event of osteogenesis. Altogether, the CC-WE scaffold delivers a favorable microenvironment to promote a forthcoming platform for bone tissue regeneration applications.

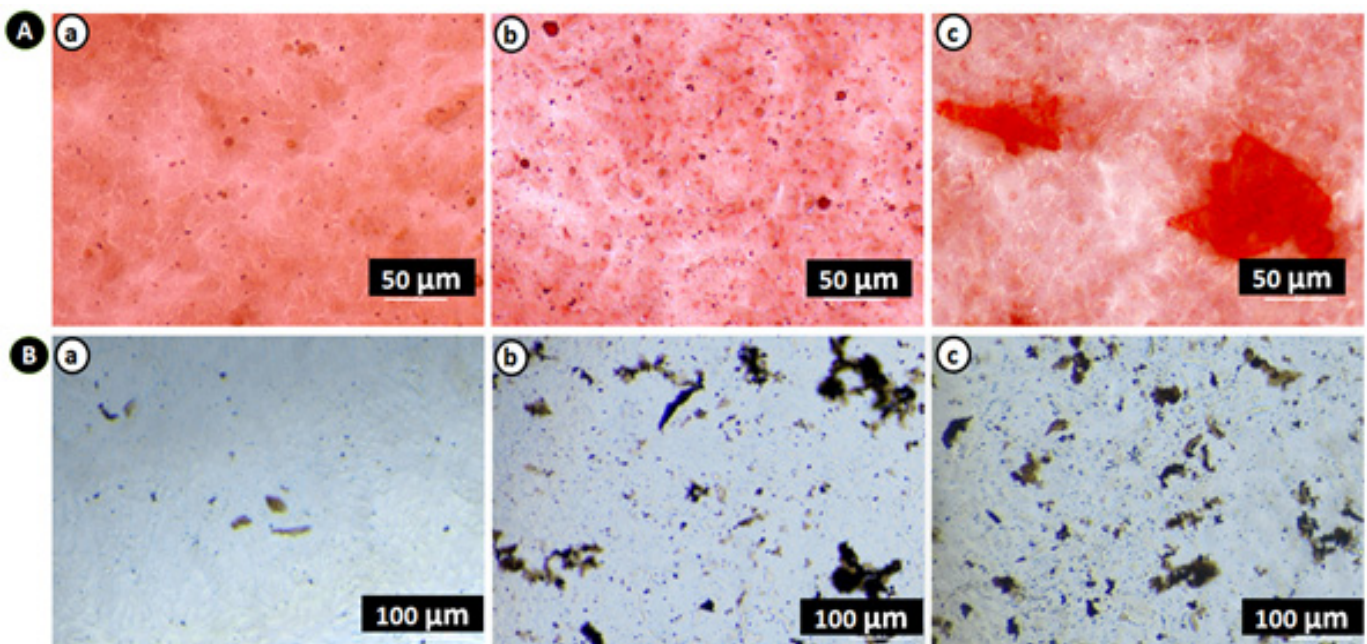


**Figure 5: Early biomineralization of the scaffolds. A (a-c) represent ARS-stained images of the control (no scaffolds), CC, and CC-WE respectively. B (a-c) denote the control (no scaffolds), CC, and CC-WE, respectively, after von Kossa staining.**

## Acknowledgements

Praseetha R. Nair gratefully acknowledges the Kerala State Council for Science, Technology and Environment (KSCSTE -WSD Back to Lab scheme), Kerala, for the financial support of this work. The authors are very much grateful to the Department of Biotechnology, CUSAT for providing their cell culture facility.

## References

1. J.Y. Park, S.H. Park, M.G. Kim, S.H. Park, T.H. Yoo, M.S. Kim, Biomimetic Scaffolds for Bone Tissue Engineering, *Adv. Exp. Med. Biol.*, 1064, 109–121 (2018).
2. L.P. Corrales, M.L. Esteves, J.A. E. Vick, Scaffold Design for Bone Regeneration, *J. Nanosci. Nanotechnol.*, 14 (1), 15–56 (2014).
3. H. Ehrlich, Chitin and Collagen as Universal and Alternative Templates in Biomineralization, 52, 661–699 (2010).
4. L. Yu, M. Wei, Biomineralization of Collagen-Based Materials for Hard Tissue Repair. *Int. J. Mol. Sci.*, 22 (2), 1–17 (2021).
5. J. Wang, C. Liu, Biomimetic Collagen/Hydroxyapatite Composite Scaffolds: Fabrication and Characterizations. *J. Bionic Eng.*, 11 (4), 600–609. (2014).
6. D. Zhang, X. Wu, J. Chen, K. Lin, The Development of Collagen Based Composite Scaffolds for Bone Regeneration. *Bioact. Mater.*, 3 (1), 129–138 (2018).
7. A. Martínez, M.D. Blanco, N. Davidenko, R.E. Cameron, Tailoring Chitosan/Collagen Scaffolds for Tissue Engineering: Effect of Composition and Different Crosslinking Agents on Scaffold Properties. *Carbohydr. Polym.*, 132, 606–619 (2015).
8. F. Croisier, C. Jérôme, Chitosan-Based Biomaterials for Tissue Engineering. *Eur. Polym. J.*, 49 (4), 780–792 (2013).
9. I.V. Yannas, D.S. Tzeranis, B.A. Harley, P. T. C. So, Biologically Active Collagen-Based Scaffolds: Advances in Processing and Characterization. *Philos. Trans. R. Soc. A Math. Phys. Eng. Sci.*, 368 2123–2139 (2010).
10. C.G. Knight, L.F. Morton, A.R. Peachey, D.S. Tuckwell, R.W. Farndale, M.J. Barnes, The Collagen-Binding  $\alpha$ -Domains of Integrins  $\alpha 1/\alpha 1$  and  $\alpha 2/\alpha 1$  Recognize the Same Specific Amino Acid Sequence, GFOGER, in Native (Triple-Helical) Collagens. *J. Biol. Chem.*, 275 (1), 35–40 (2000).
11. U. Anand, N. Jacobo-Herrera, A. Altemimi, N. Lakhssassi, A Comprehensive Review on Medicinal Plants as Antimicrobial Therapeutics: Potential Avenues of Biocompatible Drug Discovery. *Metabolites*, 9 (11), 1–13. (2019).
12. S. Siddiqui, E. Ahmad, M. Gupta, V. Rawat, N. Shivnath, M. Banerjee, M. S. Khan, M. Arshad, *Cissus Quadrangularis* Linn Exerts Dose-Dependent Biphasic Effects: Osteogenic and Anti-Proliferative, through Modulating ROS, Cell Cycle and Runx2 Gene Expression in Primary Rat Osteoblasts. *Cell Prolif.*, 48 (4), 443–454 (2015).
13. A. Shirwaikar, S. Khan, S. Malini, Antiosteoporotic Effect of Ethanol Extract of *Cissus Quadrangularis* Linn. on Ovariectomized Rat. *J. Ethnopharmacol.*, 89 (2–3), 245–250 (2003).
14. B.K. Potu, M.S. Rao, N.G. Kutty, K.M.R. Bhat, M.R. Chamallamudi, S.R. Nayak, Petroleum Ether Extract of *Cissus Quadrangularis* (Linn) Stimulates the Growth of Fetal Bone during Intra Uterine Developmental Period: A Morphometric Analysis. *Clinics*, 63 (6), 815–820 (2008).
15. R.H. Toor, S. Malik, H. Qamar, F. Batool, M. Tariq, Z. Nasir, R. Tassaduq, J.B. Lian, J.L. Stein, G.S. Stein, et al. Osteogenic Potential of Hexane and Dichloromethane Fraction of *Cissus Quadrangularis* on Murine Preosteoblast Cell Line MC3T3-E1 (Subclone 4). *J. Cell. Physiol.*, 234 (12), 23082–23096 (2019).
16. P.R. Nair, S. Sreeja, G.S. Sailaja, In Vitro Biomineralization and Osteogenesis of *Cissus Quadrangularis* Stem Extracts/: An Osteogenic Regulator for Bone Tissue Engineering. *J. of Biosci.*, 46:88 (2021).
17. P.R. Nair, S. Sreeja, G.S. Sailaja, Early Biomineralizing Chitosan–Collagen Hybrid Scaffold with *Cissus Quadrangularis* Extract for Regenerative Bone Tissue Engineering, *New J. Chem.*, 45 (42), 19733–19745, (2021).
18. T. Kokubo and Hiroaki. How Useful Is SBF in Predicting in Vivo Bone Bioactivity/? *J. Biomaterials*, 27, 2907–2915. (2006).
19. C.A. Gregory, W.G. Gunn, A. Peister, D.J. Prockop, An Alizarin Red-Based Assay of Mineralization by Adherent Cells in Culture/: Comparison with Cetylpyridinium Chloride Extraction. *Anal. Biochem.*, 329, 77–84, (2004).
20. G.S. Sailaja, K. Sreenivasan, Y. Yokogawa, T.V. Kumary, H.K. Varma, Bioinspired Mineralization and Cell Adhesion on Surface Functionalized Poly(Vinyl Alcohol) Films. *Acta Biomater.*, 5 (5), 1647–1655. (2009).
21. J. Li, H. Sun, D. Sun, Y. Yao, F. Yao, K. Yao, Biomimetic Multicomponent Polysaccharide/Nano-Hydroxyapatite Composites for Bone Tissue Engineering. *Carbohydr. Polym.*, 85 (4), 885–894 (2011).
22. C.M. Murphy, M.G. Haugh, F.J. O'Brien, The Effect of Mean Pore Size on Cell Attachment, Proliferation and Migration in Collagen-Glycosaminoglycan Scaffolds for Bone Tissue Engineering. *Biomaterials*, 31 (3), 461–466 (2010).
23. S. H. Park, E. S. Gil, H. Shib, H. J. Kima, K. Leeb, Relationships Between Degradability of Silk Scaffolds and Osteogenesis. *Bone*, 23 (1), 1–7 (2008).
24. A. Zareidoost, M. Yousefpour, The Relationship of Surface Roughness and Cell Response of Chemical Surface Modification of Titanium. *J. Mater Sci Mater Med.*, 23 (6), 1479–1488 (2012).
25. A.J. Engler, S. Sen, H.L. Sweeney, D.E. Discher, Matrix Elasticity Directs Stem Cell Lineage Specification., 677–689 (2006).
26. A. Arvidsson, F. Currie, P. Kjellin, Y.T. Sul, V. Stenport, Nucleation and Growth of Calcium Phosphates in the Presence of Fibrinogen on Titanium Implants with Four Potentially Bioactive Surface Preparations. An in Vitro Study. *J. Mater. Sci. Mater. Med.*, 20 (9), 1869–1879 (2009).
27. L.L. Fernandes, C.X. Resende, D.S. Tavares, G.A. Soares, L.O. Castro, J.M. Granjeiro, Cytocompatibility of Chitosan and Collagen-Chitosan Scaffolds for Tissue Engineering. *Polimeros*, 21 (1), 1–6 (2011).
28. S. Sreeja, C.V. Muraleedharan, P.R.H.K. Varma, G.S. Sailaja, Surface-Transformed Osteoinductive Polyethylene Terephthalate Scaffold as a Dual System for Bone Tissue Regeneration with Localized Antibiotic Delivery. *Mater. Sci. Eng. C*, 109, 110491 (2020).
29. H. Liu, H. Yazici, C. Ergun, T.J. Webster, H. Bermek, An in vitro Evaluation of the Ca/P Ratio for the Cytocompatibility of Nano-to-Micron Particulate Calcium Phosphates for Bone Regeneration. *Acta Biomater.*, 4 (5), 1472–1479 (2008).
30. S. Talebian, M. Mehrali, S. Mohan, B.H.R. Raghavendran, M. Mehrali, H. M. Khanlou, T. Kamarul, A.M. Afifi, A.A. Abass, Chitosan (PEO)/Bioactive Glass Hybrid Nanofibers for Bone Tissue Engineering. *RSC Adv.*, 4 (90), 49144–49152. (2014).